Article

Journal of Vibration and Control
2015, Vol. 21(14) 2825–2837

DOI: 10.1177/1077546313517589
jvc.sagepub.com
SAGE

Analytical and experimental investigation of overhead transmission line vibration

O Barry[1], JW Zu[1] and DCD Oguamanam[2]

Abstract

The vibration of a single-conductor transmission line with a Stockbridge damper is examined by modeling the system as a double-beam concept. The equations of motion are derived using Hamilton's principle, and expressions are presented for the frequency equation, mode shapes, and orthogonality conditions. The analytical results are validated experimentally. The effect of the damper characteristics and location on the system natural frequencies is investigated via a parametric study. The role of the latter with respect to frequency is inconclusive. The present approach enables transmission lines designers to determine the exact natural frequencies and mode shapes that are required in the study of the vibrational response of a single conductor with a Stockbridge damper.

Keywords

Stockbridge damper, Strouhal frequency, messenger

1. Introduction

The vibration of overhead transmission lines is one of the most crucial factors that contribute to power outages. This is a wind-induced high-frequency low-amplitude vibration. The frequency of vibration varies between 3 and 150 Hz and causes a peak-to-peak amplitude of up to one conductor diameter. Stockbridge dampers are often employed to eliminate or reduce this vibration. Their effectiveness is highly dependent on their overall characteristic, location, and the characteristic of the conductor.

Several authors have studied the vibration of transmission lines. The most common approach is a combination of a numerical and an experimental method (Claren and Diana, 1969; Dhotard et al., 1978; Nigol and Houston, 1985; Kraus and Hagedorn, 1991; Vecchiarelly et al., 2000; Verma and Hagerdorn, 2004; Chan and Lu, 2007). The single conductor is usually modeled as an axially loaded Euler–Bernoulli beam while the Stockbridge damper is represented by a single concentrated force on the conductor. The force is expressed in terms of the velocity of the conductor at the point of attachment of the damper and damper impedance, which are usually obtained experimentally.

An attempt to depart from the above-mentioned conventional methods of modeling a single-conductor transmission line was reported by Barry et al. (2011, 2013). Both conductor and damper were modeled as one unified system in order to account for their two-way coupling. The finite element method was used to determine the system natural frequencies and time responses. While the efficacy of the finite element model was demonstrated, the procedure was very complicated and computationally intensive. Further, the finite element method is an approximate technique. The aim of the present study was to address these shortcomings by presenting an analytical approach that yielded exact solutions (in that the equations of motion and boundary conditions are satisfied exactly) with minimal complications.

The proposed model was based on double-beam concepts. The conductor was modeled as an axially loaded Euler–Bernoulli beam and the Stockbridge damper was modeled as an Euler–Bernoulli beam with rigid tip masses. The Stockbridge damper was

[1]Department of Mechanical and Industrial Engineering, The University of Toronto, Canada
[2]Department of Mechanical and Industrial Engineering, Ryerson University, Toronto, Canada

Received: 27 July 2013; accepted: 6 November 2013

Corresponding author:
O Barry, Department of Mechanical and Industrial Engineering, The University of Toronto, Toronto, Ontario M5S 3G8, Canada.
Email: oumar.barry@utoronto.ca

arbitrarily located along the span of the conductor. Numerous studies on the vibration of double-beam/string systems abound in the literature (Yamaguchi, 1984; Oguamanam et al., 1998; Oniszczuk, 2000; Vu et al., 2000; Oniszczuk, 2003; Abu-Hilal, 2006; Foda, 2009; Palmeri and Adhikari, 2011; Foda, 2013). However, these investigations were either limited to cases where both beams were continuously connected by viscous elastic layers or where one of the beams was attached to the tip of the other.

In spite of this interest, there are no investigations where the primary beam is axially loaded and/or supporting in-span beam with tip mass. The use of this concept to analytically model a single-conductor transmission line with a Stockbridge damper was examined in this study for the first time. The equations of motion were derived using Hamilton's principle. The expressions for the characteristic equation, mode shapes, and orthogonality relations are presented. The analytical results were experimentally validated. Parametric studies were then used to examine the effect of the damper characteristics and location on the system natural frequencies.

2. Description of the system

A schematic of a single conductor with a Stockbridge damper is depicted in Figure 1. The conductor is represented as a pinned–pinned beam to delineate suspension spans. The Stockbridge damper is attached at a distance L_{c_1} and consists of a messenger (or damper cable), a mass (or counterweight) at each end of the messenger, and a clamp. This clamp is a rigid massless link with length h (this is the distance separating the conductor and the messenger). The messenger is modeled as two cantilevered beams with a tip mass at each end.

3. Equations of motion

Two reference frames were attached at the ends of the conductor as shown in Figure 1. A third reference frame was attached at the point of contact between the clamp and the messenger. The damper was attached at a distance L_{c_1} from the left-hand-side reference frame; it divided the conductor into two segments. The transverse displacement of each segment was measured relative to the appropriate reference frame, and it is denoted by $w_{ci}(x,t)$ for $i = 1, 2$. The messenger was also divided into two segments and the transverse displacement is denoted by $w_{mi}(x_m, t)$. The system kinetic $\mathcal{T}$ and potential $\mathcal{V}$ energy can be expressed as

$$\begin{aligned}\mathcal{T} =& \frac{1}{2}\sum_{i=1}^{2}\Bigg\{m_c\int_0^{L_{ci}}\dot{w}_{ci}^2\,dx + m_i\Big\{\dot{w}_{c_1}^{*2} + 2\dot{w}_{c_1}^{*}\Big((-1)^{(i+1)}\dot{w}'^{*}_{c_1}L_{mi} + \dot{w}_{mi}^{*}\Big)\\ &+\dot{w}_{c_1}{}'^{*2}\left(h^2+L_{mi}^2\right) + (-1)^{(i+1)}2L_{mi}\dot{w}_{mi}^{*}\dot{w}'^{*}_{c_1} + \dot{w}_{mi}^{*2}\Big\}\\ &+I_i\left(\dot{w}'^{*}_{c_1} + (-1)^{(i+1)}\dot{w}'^{*}_{mi}\right)^2 + m_{mi}\left(\dot{w}_{c_1}^{*2} + \left(\dot{w}'^{*}_{c_1}h\right)^2\right)\\ &+m_m\int_0^{L_{mi}}\left\{2\dot{w}_{c_1}^{*}\dot{w}_{mi} + (-1)^{(i+1)}2x_m\dot{w}'^{*}_{c_1}\dot{w}_{mi} + \dot{w}_{mi}^2\right\}dx_m\\ &+m_m\left((-1)^{(i+1)}\dot{w}_{c_1}^{*}\dot{w}'^{*}_{c_1}L_{mi}^2 + \frac{1}{3}\dot{w}'^{*2}_{c_1}L_{mi}^3\right)\Bigg\}\end{aligned} \tag{1}$$

$$\begin{aligned}\mathcal{V} =& \frac{1}{2}\sum_{i=1}^{2}\Bigg(E_cI_c\int_0^{L_{ci}}w''^2_{ci}\,dx + T\int_0^{L_{ci}}w'^2_{ci}\,dx\\ &+E_mI_m\int_0^{L_{mi}}w''^2{}_{mi}\,dx_m\Bigg)\end{aligned} \tag{2}$$

where m_1 (m_2) is the tip mass on the right-hand (left-hand) side; I_1 (I_2) is the tip rotational inertia on the right-hand (left-hand) side; L_{m_1} (L_{m_2}) is the length of the messenger on the right-hand (left-hand) side; m_c (m_m) is the mass per unit length of the conductor (messenger); m_{m1} (m_{m2}) is the mass of the messenger on the right-hand (left-hand) side; T denotes the conductor tension; E_cI_c (E_mI_m) is the flexural rigidity of the conductor (messenger); $w_{c_1}^{*}$ is the transverse displacement of the conductor evaluated at L_{c_1}; $w_{m_1}^{*}$ ($w_{m_2}^{*}$) is the transverse displacement of the right-end (left-end) counterweight; and T is the tension of the conductor. The overdots and

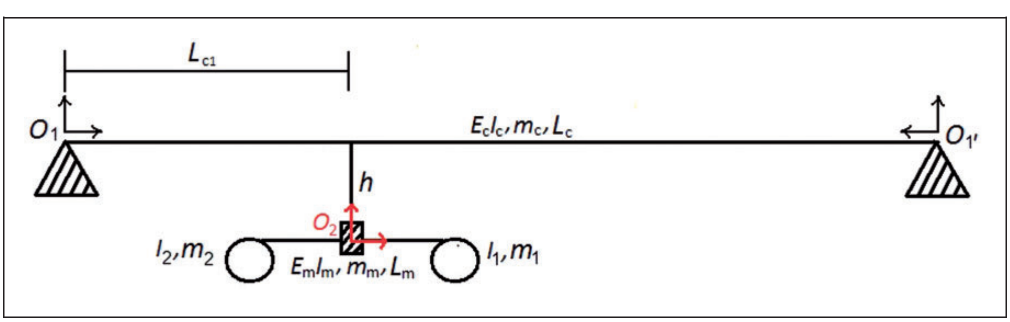

Figure 1. Schematic of a single conductor with a Stockbridge damper.

primes denote temporal and spatial derivation, respectively.

The equations of motion, equations (3) and (4), were obtained by substituting the energy expressions in Hamilton's principle and taking the variations of the field variables (δw_{c_1}, δw_{c_2}, δw_{m_1}, and δw_{m_2}),

$$m_c \ddot{w}_{ci} + E_c I_c w''''_{ci} - T w''_{ci} = 0 \tag{3}$$

$$m_m\left(\ddot{w}^*_{c_1} + (-1)^{(i+1)}\ddot{w}'^*_{c_1} L_{mi} + \ddot{w}_{mi}\right) + E_m I_m w''''_{mi} = 0 \tag{4}$$

Note that the subscript 'i' $\in [1,2]$ identifies the right-hand and left-hand segments of both the conductor and messenger. The continuity conditions of the displacement at the attachment point of the damper to the conductor, L_{c_1}, yielded the following equations:

$$w_{c_1}(L_{c_1}, t) = w_{c_2}(L_{c_2}, t) \tag{5}$$

$$w'_{c_1}(L_{c_1}, t) = -w'_{c_2}(L_{c_2}, t) \tag{6}$$

From the variation of the conductor displacement, δw_{c_1}, the obtained shear force boundary condition at the location of the damper may be written as

$$\sum_{i=1}^{2}\Big\{m_i\left(\ddot{w}^*_{c_1} + (-1)^{(i+1)}\ddot{w}'^*_{c_1} L_{mi} + \ddot{w}^*_{mi}\right) + \ddot{w}^*_{c_1} m_{mi} + m_m \int_0^{L_{mi}} \ddot{w}_{mi}\, dx_m + \frac{1}{2} m_m \ddot{w}'^*_{c_1}(-1)^{(i+1)} L^2_{mi}\Big\} - E_c I_c\left(w'''^*_{c_1} + w'''^*_{c_2}\right) + T\left(w'^*_{c_1} + w'^*_{c_2}\right) = 0 \tag{7}$$

The contributions from the tension vanished because of equation (6). The bending moment boundary condition at the attachment of the messenger may be expressed as

$$\sum_{i=1}^{2}\Big\{m_i\Big[(-1)^{(i+1)}\ddot{w}^*_{c_1} L_{mi} + w_c{}'^*(h^2 + L^2_{mi}) + (-1)^{(i+1)} L_{mi}\ddot{w}^*_{mi}\Big] + I_i\left(\ddot{w}'^*_{c_1} + (-1)^{(i+1)}\ddot{w}'^*_{mi}\right) + \ddot{w}'^*_{c_1} h^2 m_{mi} + m_m \int_0^{L_{mi}} (-1)^{(i+1)} x_m \ddot{w}_{mi}\, dx_m + \frac{1}{2} m_m\left((-1)^{(i+1)}\ddot{w}^*_{c_1} L^2_{mi} + \frac{2}{3}\ddot{w}'^*_{c_1} L^3_{mi}\right)\Big\} + E_c I_c\left(w''^*_{c_1} - w''^*_{c_2}\right) = 0 \tag{8}$$

The last set of boundary conditions for the conductor was obtained by enforcing no displacement and bending moment at both ends of each segment:

$$w_{ci}(0, t) = 0 \tag{9}$$

$$w''_{ci}(0, t) = 0 \tag{10}$$

With respect to the messenger, the shear force boundary conditions at each end, L_{m_1} and L_{m_2}, can be expressed as

$$m_i\left(\ddot{w}^*_{mi} + \ddot{w}^*_{c_1} + (-1)^{(i+1)} L_{mi}\ddot{w}'^*_{c_1}\right) - E_m I_m w'''^*_{mi} = 0 \tag{11}$$

and the bending moment boundary condition at each end is

$$I_i\left(\ddot{w}'^*_{mi} + (-1)^{(i+1)}\ddot{w}'^*_{c_1}\right) + E_m I_m w''^*_{mi} = 0 \tag{12}$$

The Stockbridge damper behaves as a cantilevered beam at the junction of the clamp and the messenger $x_m = 0$. Hence, the displacement and rotation of both the right- and left-side messengers are zero:

$$w_{mi}(0, t) = 0 \tag{13}$$

$$w'_{mi}(0, t) = 0 \tag{14}$$

4. Frequency equation and mode shapes

The transverse vibration displacement for each segment of the conductor and messenger can be expressed as

$$w_{ci}(x, t) = Y_{ci}(x) e^{i\omega t} \tag{15}$$

$$w_{mi}(x_m, t) = Y_{mi}(x) e^{i\omega t} \tag{16}$$

Substituting the above equations (equations (15) and (16)) into the equations of motion (equations (3) and (4)) yielded

$$Y''''_{ci} - S^2 Y''_{ci} - \Omega_c^4 Y_{ci} = 0 \tag{17}$$

$$Y''''_{mi} - \Omega_m^4 Y_{mi} = \Omega_m^4\left(Y^*_{c_1} + (-1)^{(i+1)} Y'^*_{c_1} x_m\right) \tag{18}$$

where

$$\Omega_c = \left(\frac{\omega^2 m_c}{E_c I_c}\right)^{\frac{1}{4}}$$

$$\Omega_m = \left(\frac{\omega^2 m_m}{E_m I_m}\right)^{\frac{1}{4}}$$

and

$$S = \sqrt{\frac{T}{E_c I_c}}$$

The solutions of the above differential equations can be expressed as

$$Y_{ci}(x) = A_{1i}\sin\alpha x + A_{2i}\cos\alpha x + A_{3i}\sinh\beta x + A_{4i}\cosh\beta x \tag{19}$$

$$Y_{mi}(x_m) = B_{1i}\sin\Omega_m x_m + B_{2i}\cos\Omega_m x_m + B_{3i}\sinh\Omega_m x_m + B_{4i}\cosh\Omega_m x_m - \left(Y^*_{c_1} + (-1)^{(i+1)} x_m Y^{*\prime}_{c_1}\right) \tag{20}$$

where

$$\alpha = \sqrt{-\frac{S^2}{2} + \sqrt{\frac{S^4}{4} + \Omega_c^4}}$$

and

$$\beta = \sqrt{\frac{S^2}{2} + \sqrt{\frac{S^4}{4} + \Omega_c^4}}$$

By applying boundary conditions at each end of the conductor, the coefficients A_{21}, A_{41}, A_{22}, and A_{42} vanished and equation (19) reduced to

$$Y_{ci}(x) = A_{1i}\sin\alpha x + A_{3i}\sinh\beta x \tag{21}$$

Substituting equation (15) in equations (5) and (6) yields

$$Y_{c_1}\left(L_{c_1}\right) = Y_{c_2}\left(L_{c_2}\right) \tag{22}$$

$$Y'_{c_1}\left(L_{c_1}\right) = -Y'_{c_2}\left(L_{c_2}\right) \tag{23}$$

Equations (15) and (16) were substituted into the shear forces boundary condition (equation (7)) at $x = L_{c_1}$, and after some algebraic manipulation yielded

$$\omega^2 \sum_{i=1}^{2} \left\{ m_i\left(Y^*_{c_1} + (-1)^{(i+1)} Y'^*_{c_1} L_{mi} + Y^*_{mi} \right) + m_{mi} Y^*_{c_1} + m_m \int_0^{L_{mi}} Y_{mi}\, dx_m + (-1)^{(i+1)} \frac{1}{2} m_m Y'^*_{c_1} L^2_{mi} \right\} \tag{24}$$

$$+E_c I_c \left(Y'''^*_{c_1} + Y'''^*_{c_2} \right) = 0 \tag{25}$$

Similarly, the bending moment boundary condition at $x = L_{c_1}$ (i.e. equation (8)) yielded

$$\begin{aligned}\omega^2 \sum_{i=1}^{2} \Bigg\{ & m_1.\left[(-1)^{(i+1)} Y^*_{c_1} L_{mi} + Y'^*_{c_1}\left(L^2_{mi} + h^2\right) + (-1)^{(i+1)} L_{mi} Y^*_{mi} \right] \\ & + I_i\left(Y'^*_{c_1} + (-1)^{(i+1)} Y^*_{mi} \right) + m_{mi} h^2 Y'^*_{c_1} \\ & + m_m \int_0^{L_{mi}} (-1)^{(i+1)} x_m w_{mi}\, dx_m \\ & + \frac{1}{2} m_m \left((-1)^{(i+1)} Y^*_{c_1} L^2_{mi} + \frac{2}{3} Y'^*_{c_1} L^3_{mi} \right) \Bigg\} \\ & - E_c I_c \left(Y''^*_{c_1} - Y''^*_{c_2} \right) = 0 \end{aligned} \tag{26}$$

For the messenger cable, equations (15) and (16) were substituted into equations (11) and (12) to obtain the following:

$$Y^*_{c_1} + (-1)^{(i+1)} L_{mi} Y_{c_1}{}' + Y^*_{mi} + \lambda_{mi} Y'''^*{}_{mi} = 0 \tag{27}$$

$$(-1)^{(i+1)} Y'^*_{c_1} + Y'^*_{mi} - \kappa_{mi} Y''^*_{mi} = 0 \tag{28}$$

where

$$\lambda_{mi} = \frac{E_m I_m}{m_i \omega^2}$$

$$\kappa_{mi} = \frac{E_m I_m}{I_i \omega^2}$$

Equations (13) and (14) naturally reduced to

$$Y_{mi}(0) = 0 \tag{29}$$

$$Y'_{mi}(0) = 0 \tag{30}$$

A set of 12 algebraic homogeneous equations (four are from the conductor and eight from the messenger) was obtained by substituting equations (20) and (21) into equations (22) to (30). These algebraic equations are linear in the unknown coefficients (As and Bs) and can be written in matrix format as

$$[\mathcal{F}]_{12\times 12}\{q\}_{12\times 12} = \{0\}_{12\times 12} \tag{31}$$

where the elements of the matrix $\mathcal{F}$ are listed in the appendix and

$q = [A_{11}, A_{31}, A_{12}, A_{32}, B_{11}, B_{21}, B_{31}, B_{41}, B_{12}, B_{22}, B_{32}, B_{42}]^T$, with the superscript T denoting transposition. A nontrivial solution to the equation is possible when matrix $\mathcal{F}$ is singular. Hence, the characteristic or frequency equation was obtained as

$$\det([\mathcal{F}]_{12\times 12}) = 0 \tag{32}$$

The mode shapes of the conductor were deduced by using equation (22) while ignoring the hyperbolic function terms since the tension and the span length in transmission lines are usually very high. Assuming that $A_{11} = 1$, the conductor mode shapes for each segment can be expressed as

$$Y_{c_1}(x) = \sin \alpha x_1 \tag{33}$$

$$Y_{c_2}(x) = \frac{s_1}{s_2} \sin \alpha x_2 \tag{34}$$

The mode shapes of the messenger were derived by using the shear and moment conditions at each end of the messenger (equations (27) and (28)), and the displacement and slope at the clamp (equations (29) and (30)). With reference to equation (20), the coefficients of the mode shapes of the messenger are

$$\begin{aligned} B_{1\mathrm{i}} = \frac{1}{\lambda_\mathrm{i}} \Big\{ & \mathcal{F}_{11,1}\mathcal{F}_{(\mathrm{i}+4),7}\mathcal{F}_{(\mathrm{i}+6),8} - \mathcal{F}_{11,1}\mathcal{F}_{(\mathrm{i}+4),7}\mathcal{F}_{(\mathrm{i}+6),6} \\ & + \mathcal{F}_{1,1}\mathcal{F}_{(\mathrm{i}+4),6}\mathcal{F}_{(\mathrm{i}+6),8} - \mathcal{F}_{1,1}\mathcal{F}_{(\mathrm{i}+4),8}\mathcal{F}_{(\mathrm{i}+6),6} \\ & - \mathcal{F}_{11,1}\mathcal{F}_{(\mathrm{i}+4),8}\mathcal{F}_{(\mathrm{i}+6),7} + \mathcal{F}_{11,1}\mathcal{F}_{(\mathrm{i}+4),6}\mathcal{F}_{(\mathrm{i}+6),7} \Big\} \end{aligned} \tag{35}$$

$$\begin{aligned} B_{2\mathrm{i}} = -\frac{1}{\lambda_\mathrm{i}} \Big\{ & -\mathcal{F}_{1,1}\mathcal{F}_{(\mathrm{i}+6),8}\mathcal{F}_{(\mathrm{i}+4),7} + \mathcal{F}_{1,1}\mathcal{F}_{(\mathrm{i}+6),8}\mathcal{F}_{(\mathrm{i}+4),5} \\ & + \mathcal{F}_{1,1}\mathcal{F}_{(\mathrm{i}+6),7}\mathcal{F}_{(\mathrm{i}+4),8} - \mathcal{F}_{1,1}\mathcal{F}_{(\mathrm{i}+6),5}\mathcal{F}_{(\mathrm{i}+4),8} \\ & - \mathcal{F}_{11,1}\mathcal{F}_{(\mathrm{i}+6),5}\mathcal{F}_{(\mathrm{i}+4),7} + \mathcal{F}_{11,1}\mathcal{F}_{(\mathrm{i}+6),7}\mathcal{F}_{(\mathrm{i}+4),5} \Big\} \end{aligned} \tag{36}$$

$$\begin{aligned} B_{3\mathrm{i}} = -\frac{1}{\lambda_\mathrm{i}} \Big\{ & \mathcal{F}_{11,1}\mathcal{F}_{(\mathrm{i}+6),8}\mathcal{F}_{(\mathrm{i}+4),5} - \mathcal{F}_{11,1}\mathcal{F}_{(\mathrm{i}+6),6}\mathcal{F}_{(\mathrm{i}+4),5} \\ & + \mathcal{F}_{1,1}\mathcal{F}_{(\mathrm{i}+4),6}\mathcal{F}_{(\mathrm{i}+6),8} - \mathcal{F}_{1,1}\mathcal{F}_{(\mathrm{i}+4),8}\mathcal{F}_{(\mathrm{i}+6),6} \\ & - \mathcal{F}_{11,1}\mathcal{F}_{(\mathrm{i}+6),5}\mathcal{F}_{(\mathrm{i}+4),8} + \mathcal{F}_{11,1}\mathcal{F}_{(\mathrm{i}+6),5}\mathcal{F}_{(\mathrm{i}+4),6} \Big\} \end{aligned} \tag{37}$$

$$\begin{aligned} B_{4\mathrm{i}} = \frac{1}{\lambda_\mathrm{i}} \Big\{ & -\mathcal{F}_{11,1}\mathcal{F}_{(\mathrm{i}+6),5}\mathcal{F}_{(\mathrm{i}+4),7} - \mathcal{F}_{1,1}\mathcal{F}_{(\mathrm{i}+6),6}\mathcal{F}_{(\mathrm{i}+4),7} \\ & + \mathcal{F}_{1,1}\mathcal{F}_{(\mathrm{i}+6),6}\mathcal{F}_{(\mathrm{i}+4),5} + \mathcal{F}_{11,1}\mathcal{F}_{(\mathrm{i}+6),7}\mathcal{F}_{(\mathrm{i}+4),5} \\ & + \mathcal{F}_{1,1}\mathcal{F}_{(\mathrm{i}+6),7}\mathcal{F}_{(\mathrm{i}+4),6} - \mathcal{F}_{1,1}\mathcal{F}_{(\mathrm{i}+6),5}\mathcal{F}_{(\mathrm{i}+4),6} \Big\} \end{aligned} \tag{38}$$

where the corresponding $\mathcal{F}_{\mathrm{i,j}}$ are listed in the appendix and

$$\begin{aligned} \lambda_\mathrm{i} = & \mathcal{F}_{(\mathrm{i}+6),8}\mathcal{F}_{(\mathrm{i}+4),7} - \mathcal{F}_{(\mathrm{i}+6),8}\mathcal{F}_{(\mathrm{i}+4),5} - \mathcal{F}_{(\mathrm{i}+6),6}\mathcal{F}_{(\mathrm{i}+4),7} \\ & + \mathcal{F}_{(\mathrm{i}+6),8}\mathcal{F}_{(\mathrm{i}+4),5} - \mathcal{F}_{(\mathrm{i}+6),7}\mathcal{F}_{(\mathrm{i}+4),8} + \mathcal{F}_{(\mathrm{i}+6),7}\mathcal{F}_{(\mathrm{i}+4),6} \\ & + \mathcal{F}_{(\mathrm{i}+6),5}\mathcal{F}_{(\mathrm{i}+4),8} - \mathcal{F}_{(\mathrm{i}+6),5}\mathcal{F}_{(\mathrm{i}+4),6} \end{aligned}$$

5. Orthogonality condition

After some algebraic manipulation the first orthogonality relation can be expressed as

$$\begin{aligned} & \sum_{i=1}^{2} \Big\{ m_\mathrm{c} \int_0^{L_\mathrm{ci}} Y_\mathrm{ci}^{(r)} Y_\mathrm{ci}^{(s)} dx + m_\mathrm{m} \int_0^{L_\mathrm{mi}} Y_\mathrm{mi}^{(r)} Y_\mathrm{mi}^{(s)} dx_\mathrm{m} \\ & + Y_{\mathrm{c}_1}^{(r)^*} Y_{\mathrm{c}_1}^{(s)^*} (m_\mathrm{i} + m_\mathrm{m} L_\mathrm{mi}) + Y_{\mathrm{c}_1}^{(r)^{*\prime}} Y_{\mathrm{c}_1}^{(s)^{*\prime}} \big[m_\mathrm{i} (L_\mathrm{mi}^2 + h^2) \\ & + I_\mathrm{i} + h^2 m_\mathrm{m} L_\mathrm{mi} + \frac{1}{3} L_\mathrm{mi}^3 \big] + Y_\mathrm{mi}^{(r)^*} Y_\mathrm{mi}^{(s)^*} m_\mathrm{mi} \\ & + Y_\mathrm{mi}^{(r)^{*\prime}} Y_\mathrm{mi}^{(s)^{*\prime}} I_\mathrm{i} + (-1)^{(\mathrm{i}+1)} m_\mathrm{i} L_\mathrm{mi} \Big(Y_{\mathrm{c}_1}^{(r)^{*\prime}} Y_{\mathrm{c}_1}^{(s)^*} + Y_{\mathrm{c}_1}^{(r)^*} Y_{\mathrm{c}_1}^{(s)^{*\prime}} \Big) \\ & + m_\mathrm{mi} \Big(Y_{\mathrm{c}_1}^{(r)^*} Y_\mathrm{mi}^{(s)^*} + Y_{\mathrm{c}_1}^{(s)^*} Y_\mathrm{mi}^{(r)^*} \Big) + m_\mathrm{m} \int_0^{L_\mathrm{mi}} \Big(Y_{\mathrm{c}_1}^{(r)^*} Y_\mathrm{mi}^{(s)^*} \\ & + Y_{\mathrm{c}_1}^{(s)^*} Y_\mathrm{mi}^{(r)^*} \Big) dx_\mathrm{m} + (-1)^{(\mathrm{i}+1)} \frac{1}{2} m_\mathrm{m} L_\mathrm{mi}^2 \Big(Y_{\mathrm{c}_1}^{(r)^*} Y_{\mathrm{c}_1}^{(s)^{*\prime}} + Y_{\mathrm{c}_1}^{(s)^*} Y_{\mathrm{c}_1}^{(r)^{*\prime}} \Big) \\ & + (-1)^{(\mathrm{i}+1)} m_\mathrm{i} L_\mathrm{mi} \Big(Y_{\mathrm{c}_1}^{(r)^{*\prime}} Y_\mathrm{mi}^{(s)^*} + Y_{\mathrm{c}_1}^{(s)^{*\prime}} Y_\mathrm{mi}^{(r)^*} \Big) + (-1)^{(\mathrm{i}+1)} I_\mathrm{i} \Big(Y_{\mathrm{c}_1}^{(r)^{*\prime}} Y_\mathrm{mi}^{(s)^{*\prime}} \\ & + Y_{\mathrm{c}_1}^{(s)^{*\prime}} Y_\mathrm{mi}^{(r)^{*\prime}} \Big) + (-1)^{(\mathrm{i}+1)} m_\mathrm{m} \int_0^{L_\mathrm{mi}} x_\mathrm{m} \Big(Y_{\mathrm{c}_1}^{(r)^{*\prime}} Y_\mathrm{mi}^{(s)} + Y_{\mathrm{c}_1}^{(s)^{*\prime}} Y_\mathrm{mi}^{(r)} \Big) dx_\mathrm{m} \Big\} \\ & = \delta_\mathrm{rs} \end{aligned} \tag{39}$$

where δ_rs is the Kronecker delta. The second orthogonality relation can be expressed as

$$\begin{aligned} \sum_{i=1}^{2} \Bigg(& \int_0^{L_\mathrm{ci}} Y_\mathrm{ci}^{(r)''} Y_\mathrm{ci}^{(s)''} dx - S^2 \int_0^{L_\mathrm{ci}} Y_\mathrm{ci}^{(r)'} Y_\mathrm{ci}^{(s)'} dx \\ & + \frac{E_\mathrm{m} I_\mathrm{m}}{E_\mathrm{c} I_\mathrm{c}} \int_0^{L_\mathrm{mi}} Y_\mathrm{mi}^{(r)''} Y_\mathrm{mi}^{(s)''} dx \Bigg) = \delta_\mathrm{rs} \end{aligned} \tag{40}$$

6. Experimental procedure

Two sets of experiments were conducted to validate the model. The first was performed at a conductor tension of 27.84 kN and the second, at 34.8 kN. The conductor was 795 KCMIL (Drake). (This conductor is constructed with 26 aluminum strands and seven galvanized steel wires as the core.) The material properties and geometric parameters of the conductor and the Stockbridge damper are tabulated in Table 1. The schematic of the test set-up is depicted in Figure 2 and a photograph of the electromagnetic shaker (Bruel & Kjaer 4802) connected to the conductor is shown in Figure 3. The conductor was suspended from two steel-reinforced concrete blocks (towers) with a span length of 27.25 m. Insulator clamps were used to attach the conductor to the towers through strain links. This was done in such a way as to replicate pinned–pinned boundary conditions for the conductor. A Stockbridge damper was attached to the conductor at a distance L_{c_1}.

The conductor was loaded in tension using a hydraulic ram cylinder. A load cell (Daytronics 3170) was attached at one end of the conductor to monitor the tension. The electrodynamic shaker (Bruel & Kjaer 4802) was installed at mid-span to drive the system according to the signal generated by the vibration controller. This shaker was only applicable to frequencies greater than 10 Hz. The delivered force and the velocity from the shaker were measured by a strain-gauge load cell (Dytran 106V1) and an accelerometer (B & K 4382), respectively.

Table 1. Damper parameter.

Parameter	
h	0.05 m
m_1	3.4 kg
m_2	1.46 kg
I_1	0.0175 kgm^2
I_2	0.015 kgm^2
$E_m I_m$	31.8 Nm^2
L_{m_1}	0.3 m
L_{m_2}	0.22 m
m_m	0.25 kg/m

The conductor was excited at frequencies between 10 and 45 Hz in order to determine the resonant frequencies of the conductor–damper system. A dynamic signal analyzer (PCI-6034E) was used for signal processing and data acquisition functions. The system natural frequencies were identified from frequency response curves that were obtained from the signal analyzer. These natural frequencies are tabulated in Table 2.

7. Numerical simulation

The numerical simulations were based on the material properties and parameters listed in Table 1. The length of the conductor is $L_c = 27.25$ m, with flexural rigidity $E_c I_c = 1602$ Nm^2, and linear mass density $m_c = 1.628$ kg/m.

The analytical natural frequencies were determined by numerically solving for the roots of the frequency equation (equation (32)) using the bisection method in MATLAB. The first 20 natural frequencies are displayed in Table 2 for the two tensions (27.84 kN and 34.8 kN) employed in the experiments. The Stockbridge damper was attached at a distance $L_{c_1} = 0.94$ m and $L_{c_1} = 0.88$ m for $T = 27.84$ kN and $T = 34.8$ kN, respectively.

The first six experimental modes are not shown because the shaker used to excite the conductor was

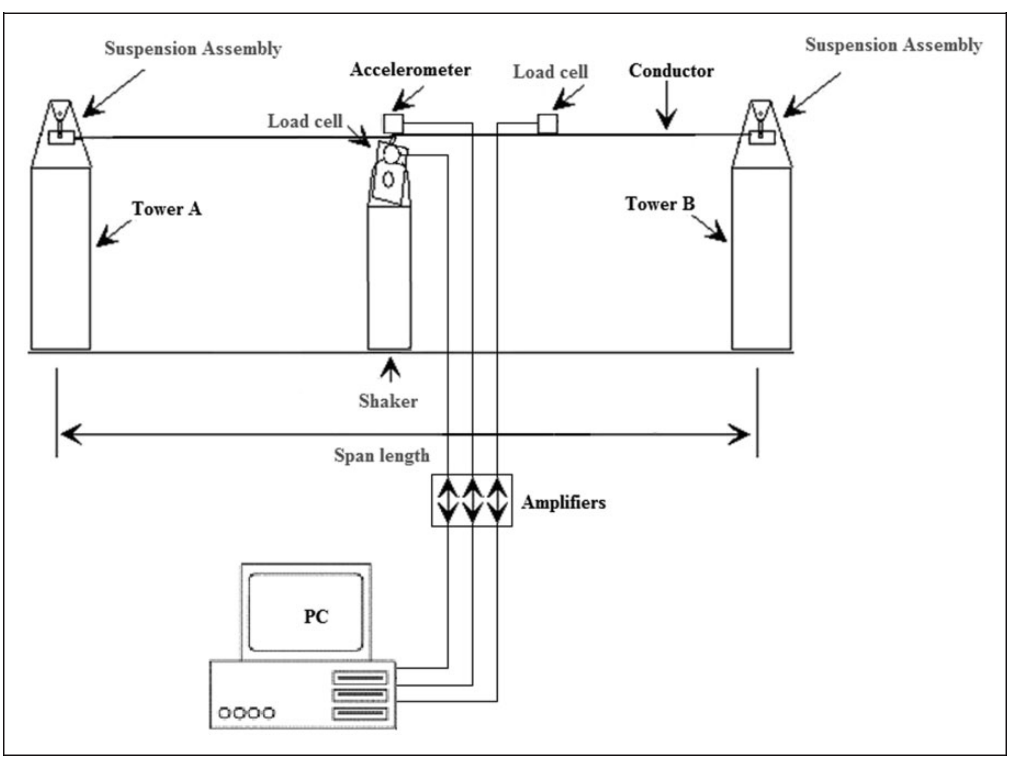

Figure 2. Schematic of experimental set-up.

only applicable for frequencies higher than 10 Hz. A comparison of the analytical and experimental data shows very good agreement. Table 2 also shows the results of the finite element method from Barry et al. (2011). These are also in good agreement with experimentally obtained resonant frequencies, but with a 2% margin of error which is slightly higher than those of the analytical method.

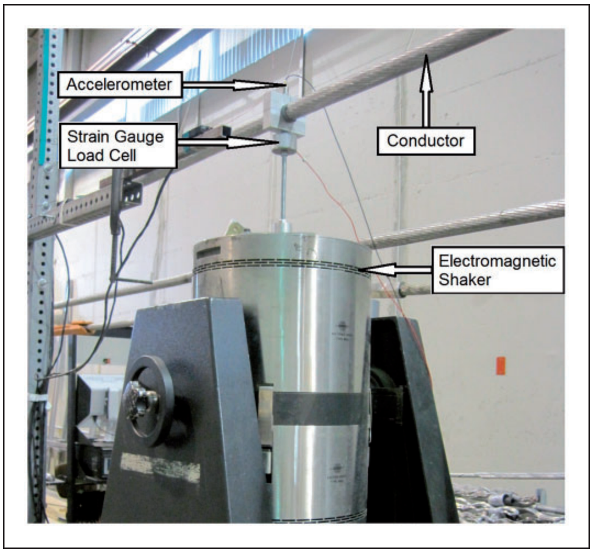

Figure 3. Photograph of the conductor, shaker, load cell, and accelerometer.

The discrepancies between the experimental and analytical results could be partly attributed to the difficulty in replicating the boundary conditions during the experiments. However, it suffices to mention that not only were the analytical results more accurate than those of the finite element; the analytical procedure was less computationally intensive and had faster execution time.

Figures 4 and 5 are depictions of the first five mode shapes of the conductor for $T = 27.84$ kN and $T = 34.8$ kN, respectively. Similarly, Figures 6 and 7 depict the first five mode shapes of the damper for $T = 27.84$ kN and $T = 34.8$ kN, respectively. Figures 4 and 5 show that the mode shapes of this system are very similar to those of a pinned–pinned beam, but the nth mode of the former corresponds to the $(n-1)^{\text{th}}$ mode of the latter.

With respect to Figures 6 and 7, the first mode of the Stockbridge damper remained relatively unchanged. This implies that the system's first mode had very little participation from the damper. The remaining four modes behaved more like a cantilevered beam.

Table 2. Validation of natural frequencies (Hz).

Mode	$T = 27.84$ kN			$T = 34.8$ kN		
	Exp.	Anal.	Ref. (Barry et al., 2011)	Exp.	Anal.	Ref. (Barry et al., 2011)
1	–	2.3953	2.3978	–	2.6780	2.6810
2	–	4.4008	4.4157	–	4.5402	4.5482
3	–	4.9556	4.9794	–	5.4390	5.4587
4	–	7.2560	7.2961	–	8.0807	8.1245
5	–	9.3722	9.4257	–	9.6785	9.7360
6	–	9.9441	10.0120	–	10.8620	10.9407
7	12.0956	12.1634	12.2593	13.0749	13.5217	13.6277
8	14.3910	14.5642	14.6818	15.5104	16.1901	16.3273
9	16.5942	16.9498	17.1010	17.5942	18.8053	18.9801
10	19.1878	19.2874	19.4680	20.8396	21.2930	21.4932
11	21.1717	21.5661	21.7955	22.7073	23.6093	23.8500
12	23.6302	23.8280	24.0862	24.5587	25.9045	26.1695
13	25.3417	26.1201	26.4206	27.0885	28.2907	28.6355
14	27.7020	28.3588	28.7044	27.7641	30.5914	30.9642
15	29.3096	30.3524	30.7484	31.4490	32.7797	33.1814
16	31.4913	32.4137	32.8581	34.0577	35.2503	35.8622
17	33.8856	34.8828	35.3717	36.5584	38.0422	38.8023
18	36.6252	37.5991	38.1732	40.0444	41.0131	41.8586
19	39.3756	40.4481	41.0821	42.6807	44.0936	45.0250
20	42.6673	43.3869	44.1125	45.7943	47.2564	48.2937

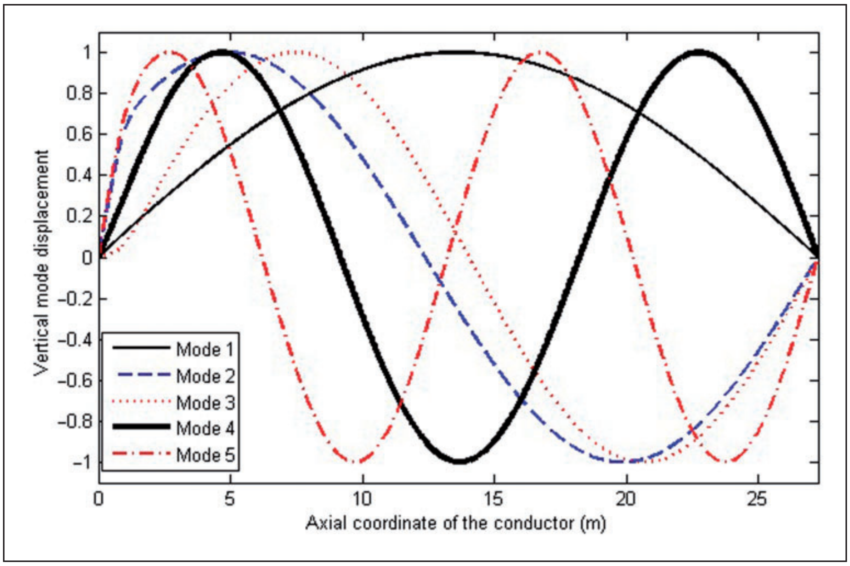

Figure 4. Conductor mode shapes for $T = 27.84$ kN.

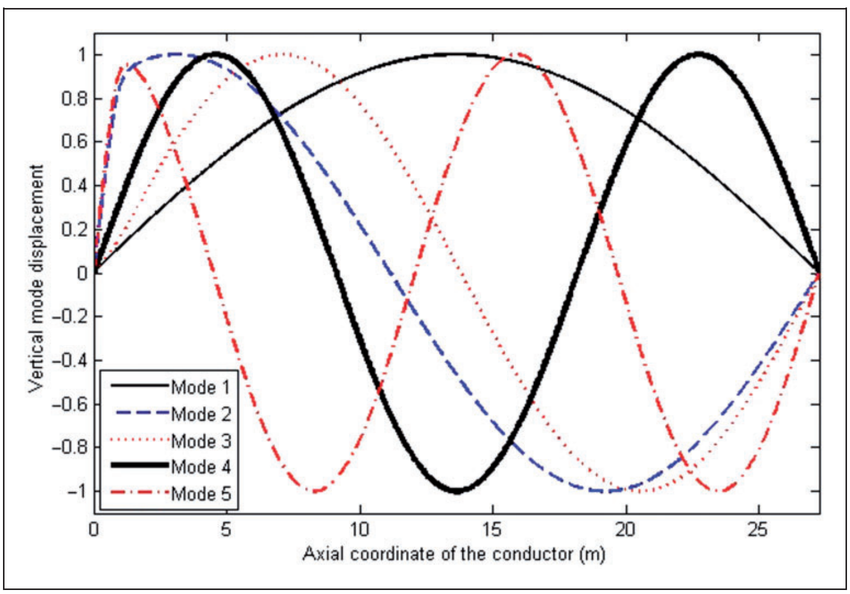

Figure 5. Conductor mode shapes for $T = 34.8$ kN.

In both Figures 6 and 7, the second mode was similar to the third except that the former deflected upward and the latter downward. Note that only the right segment of the messenger (L_{m_1}) was excited by the second and third modes. This implies that the second and third modes of the system must be closer to that of the right-side segment of the messenger.

In light of the good agreement between the analytical and experimental results, the model was used to parametrically investigate the influence of the damper characteristics and location on the system natural frequencies. Unless otherwise specified, the set of material properties are as tabulated in Table 1 and the damper was attached at a distance $L_{c_1} = 0.94$ m. The conductor tension $T = 27.84$ kN was employed in the remainder of the numerical analyses.

At the first stage of the parametric studies, the effect of the damper counterweights on the natural frequency was examined. The mass of each counterweight was varied from 0.5 kg to 4.5 kg. The results are tabulated in Table 3. As expected, the natural frequencies generally increased with decreasing total mass. However, the

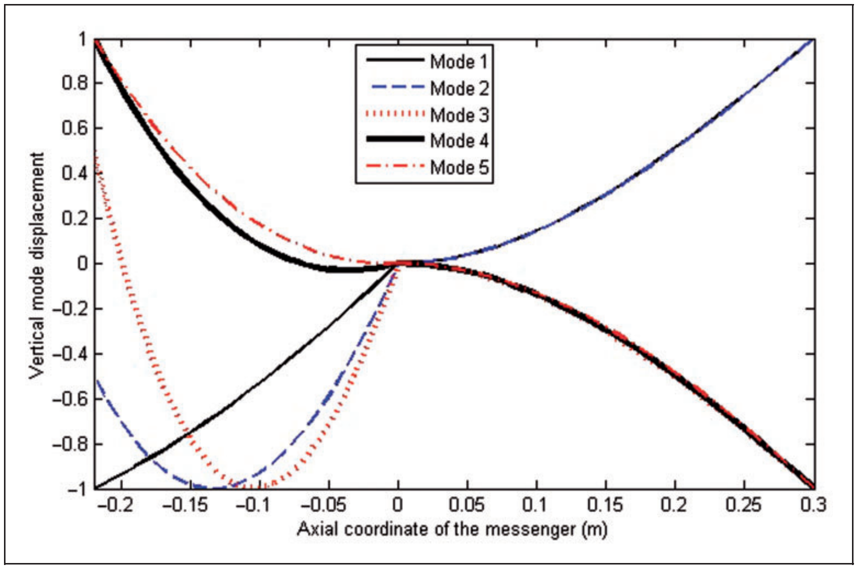

Figure 6. Messenger mode shapes for $T = 27.84\,\text{kN}$.

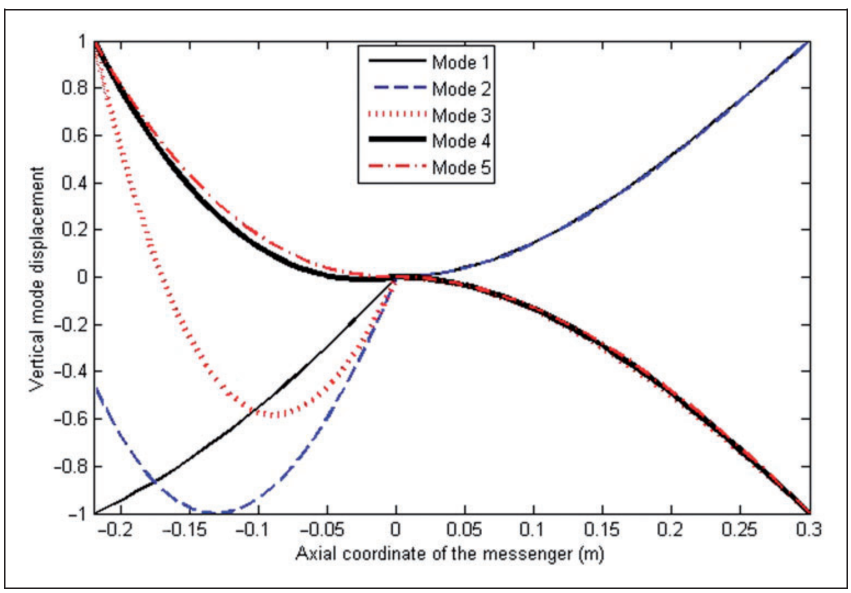

Figure 7. Messenger mode shapes for $T = 34.8\,\text{kN}$.

fundamental frequency was unchanged, which indicates that the mass of the counterweights had minimal or no effect on the first mode.

The length of the messenger on either side was varied from 0.1 to 2 m in order to examine the role of the messenger on the system natural frequencies. The obtained frequencies are tabulated in Table 4. It was observed that the natural frequencies generally decreased with increasing total length of the messenger as expected. This decrease in the natural frequency was significant even for the fundamental mode.

The system natural frequencies for varying messenger flexural rigidity are tabulated in Table 5. The results showed that the system natural frequencies generally increased with increasing flexural rigidity of the messenger. The role of the distance separating the conductor and the messenger (i.e. length of the rigid link, h) was inferred from the results tabulated in Table 6. It was observed that the natural frequencies decreased with increasing rigid link length. This decrease in the natural frequencies was less significant for the fundamental mode. Hence, the first mode was again

Table 3. Effect of counterweight masses on natural frequencies (Hz).

m_2 (kg)	Mode	m_1 (kg) 0.5	1.5	2.5	3.5	4.5
0.5	1	2.40020	2.39890	2.39730	2.39550	2.3932
	2	4.79960	4.77770	4.69650	4.36200	3.9500
	3	7.1849	6.3439	5.2991	4.9421	4.8820
	4	9.0107	7.3384	7.2819	7.2706	7.2658
	5	9.7874	9.6910	9.6842	9.6817	9.6804
1.5	1	2.3998	2.3985	2.3969	2.3950	2.3927
	2	4.7955	4.7730	4.6905	4.3573	3.9473
	3	7.1608	6.3327	5.2977	4.9415	4.8803
	4	8.9226	7.3285	7.2665	7.2540	7.2487
	5	9.4923	9.3299	9.3221	9.3194	9.3180
2.5	1	2.3994	2.3981	2.3965	2.3946	2.3923
	2	4.7900	4.7667	4.6823	4.3512	3.9440
	3	7.0752	6.3089	5.2958	4.9406	4.8778
	4	7.9269	7.2867	7.2046	7.1883	7.1814
	5	9.0748	7.9465	7.9421	7.9410	7.9405
3.5	1	2.3989	2.3976	2.3960	2.3941	2.3917
	2	4.7818	4.7574	4.6708	4.3432	3.9399
	3	6.6605	6.2365	5.2925	4.9394	4.8742
	4	7.3770	7.4215	6.7693	6.7496	6.7420
	5	9.0535	9.7449	7.4037	7.4005	7.3991
4.5	1	2.3984	2.3971	2.3955	2.3936	2.3912
	2	4.7688	4.7428	4.6534	4.3323	3.9347
	3	6.0751	5.9722	5.2862	4.9374	4.8684
	4	7.2875	6.5338	6.1599	6.1329	6.1247
	5	9.0472	7.3791	7.3444	7.3377	7.3348

Table 4. Effect of the messenger length on natural frequencies (Hz).

L_{m_2} (m)	Mode	L_{m_1} (m) 0.1	0.5	1.0	1.5	2.0
0.1	1	2.3974	2.2127	0.8142	0.4441	0.2879
	2	4.7748	2.4302	2.4014	2.4006	2.4003
	3	7.0904	4.8114	4.8021	4.8000	4.7963
	4	9.2496	7.2121	7.2000	7.1905	5.9484
	5	11.2051	9.6054	9.5864	8.7283	7.2106
0.5	1	2.3978	2.2131	0.8142	0.4441	0.2879
	2	3.3700	2.4303	2.4017	2.4010	2.4006
	3	4.7838	3.3705	3.3705	3.3705	3.3705
	4	7.1251	4.8181	4.8093	4.8073	4.8037
	5	9.3573	7.2330	7.2220	7.2132	5.9493
1	1	1.2277	1.2277	0.8142	0.4441	0.2879
	2	2.3982	2.2132	1.2278	1.2277	1.2277
	3	4.7821	2.4305	2.4021	2.4014	2.4010
	4	7.1236	4.8170	4.8080	4.8060	4.8025
	5	9.3550	7.2323	7.2212	7.2124	5.9494
1.5	1	0.6669	0.6669	0.6669	0.4441	0.2879
	2	2.3982	2.2133	0.8142	0.6669	0.6669
	3	4.7821	2.4305	2.4022	2.4014	2.4010
	4	7.1225	4.8169	4.8080	4.8060	4.8025
	5	9.1100	7.2316	7.2206	7.2118	5.9494
2	1	0.4303	0.4303	0.4303	0.4302	0.2879
	2	2.3982	2.2133	0.8142	0.4441	0.4303
	3	4.7819	2.4305	2.4022	2.4014	2.4010
	4	6.1271	4.8168	4.8079	4.8059	4.8023
	5	7.1264	6.1282	6.1282	6.1282	5.9493

Table 5. Effect of the messenger flexural rigidity on natural frequencies (Hz).

Mode	$E_m I_m$ (N/m^2) 0.1	1.0	10.0	100.0	1000.0
1	0.2879	0.8401	2.3789	2.3960	2.3964
2	0.5584	1.7632	2.6331	4.7469	4.7648
3	1.4704	2.4011	4.8047	6.6457	7.0474
4	2.1441	4.5985	5.5119	7.7690	9.1409
5	2.4025	4.8340	7.2300	9.8956	11.1076
6	4.8084	6.6791	9.6239	12.2451	13.2615
7	7.2255	7.2749	11.9507	14.4064	15.6416
8	9.6584	9.6814	13.7546	15.7283	18.1520
9	12.1122	12.1347	15.0584	17.5826	20.7434
10	14.5919	14.6161	17.1461	19.9560	23.3944
11	17.1023	17.1291	19.1027	22.4036	26.0685
12	19.6471	19.6788	20.7019	24.8682	27.9504
13	22.2253	22.2699	22.8631	27.3596	29.1293
14	24.6928	24.9075	25.3697	29.9151	31.8609
15	25.2733	27.5963	28.0008	32.5680	34.7620
16	27.6107	30.3412	30.7104	35.3305	37.7451
17	30.3395	33.1465	33.4880	38.1991	40.8034
18	33.1390	36.0166	36.3326	41.1655	43.9358
19	36.0042	38.9553	39.2457	44.2177	47.1413
20	38.9355	41.9662	42.2303	47.3172	50.4171

Table 6. Effect of clamp height on natural frequencies (Hz).

	h (m)				
Mode	0.01	0.5	1.0	1.5	2.0
1	2.3950	2.3940	2.3907	2.3840	2.3713
2	4.3574	4.3452	4.2975	4.1569	3.7714
3	4.9415	4.9409	4.9385	4.9307	4.8745
4	7.2541	7.2371	7.0962	5.9075	5.0666
5	9.3194	9.3167	8.5572	7.4561	7.3783
6	9.9127	9.8458	9.3371	9.3269	9.3257
7	12.1632	12.0116	10.3493	10.1209	10.0857
8	14.5646	14.2654	12.5256	12.4019	12.3754
9	16.9490	16.4393	14.8943	14.8146	14.7947
10	19.2828	18.5509	17.2439	17.1882	17.1731
11	21.5550	20.3939	19.4821	19.4509	19.4421
12	23.8115	21.7886	21.6128	21.6056	21.6034
13	26.1005	23.8115	23.8115	23.8115	23.8115
14	28.3314	26.1456	26.1265	26.1246	26.1240
15	30.3150	28.3625	28.3521	28.3509	28.3505
16	32.3899	30.3337	30.3287	30.3281	30.3278
17	34.8730	32.5772	32.5357	32.5300	32.5281
18	37.5963	35.1854	35.1246	35.1158	35.1128
19	40.4486	37.9646	37.8995	37.8898	37.8866
20	43.3881	40.8243	40.7631	40.7538	40.7507

Table 7. Effect of damper location on natural frequencies (Hz).

	L_{c_1}				
Mode	$L_c/100$	$L_c/10$	$L_c/6$	$L_c/4$	$L_c/2$
1	2.3999	2.3614	2.3049	2.2288	2.1201
2	4.5444	4.0203	3.9004	3.9544	4.7092
3	4.8621	5.1583	5.3589	5.4976	4.8423
4	7.2383	7.1893	7.0885	7.0926	7.0949
5	9.6696	8.8023	9.0209	9.6194	9.6104
6	12.1225	10.3922	10.7470	12.2225	9.8972
7	14.5983	14.5833	12.2794	14.5632	12.4048
8	17.0988	16.9846	14.6115	17.0170	14.6111
9	19.6190	19.5491	17.0247	19.6732	16.8610
10	22.1239	22.2159	19.2416	21.7401	19.6731
11	24.3187	24.8734	21.6055	23.9078	21.5417
12	25.6735	25.8659	24.3172	26.7988	24.8785
13	27.8490	27.8460	27.0319	27.9871	25.7063
14	30.4769	30.5062	27.7439	30.3646	28.3762
15	33.1860	32.6745	30.3640	32.9017	30.3669
16	35.7006	34.7148	33.1236	34.7440	32.4379
17	37.1094	37.4496	34.7936	38.0303	36.0100
18	39.3438	40.4795	37.3504	41.5599	37.0541
19	42.2444	43.6002	40.5902	42.1458	41.4734
20	45.2944	46.6673	42.2288	45.5969	42.0975

(continued)

Table 7. Continued

dominated by the conductor characteristics. Table 7 shows the influence of the location of the Stockbridge damper on the system natural frequencies. The location of the damper affected all five modes, but with no obvious trend.

8. Conclusions

A double-beam-concept-based analytical model was presented for the free vibration analysis of a single conductor transmission line with a Stockbridge damper for the first time. The first or main beam was subjected to an axial load and had pinned–pinned boundary conditions in order to simulate single conductor transmission lines on suspension-spans. The Stockbridge damper was modeled by an in-span beam with tip mass at each end. The model was validated experimentally. Expressions were presented for the frequency equation, mode shapes, and orthogonality relations. Experiments were conducted to validate the proposed model and the results showed very good agreement.

Parametric investigations indicated that the mass of the counterweights, length of the rigid link, length of the messenger, and flexural rigidity had more effect on the higher modes. The first mode was dominated by the conductor characteristics. The role of the location of the Stockbridge damper with respect to the system natural frequencies was inconclusive.

Acknowledgments

The authors are grateful to Andrew Rizzetto and Dmitry Ladin of Kinectrics Inc., Toronto, for their assistance with the experiments.

Funding

The financial assistance from Hydro One Inc. is acknowledged.

References

Abu-Hilal M (2006) Dynamic response of a double Euler-Bernoulli beam due to a moving constant load. *Journal of Sound and Vibration* 297: 477–491.

Barry O, Oguamanam DCD and Lin DC (2011) Free vibration analysis of a single conductor with a Stockbridge damper. In: *Proceedings of the 23rd CANCAM*, Vancouver, BC, 5–9 June 2011.

Barry O, Oguamanam DCD and Lin DC (2013) Aeolian vibration of a single conductor with a Stockbridge damper. *IMechE: Part C, Journal of Mechanical Engineering Science* 227(5): 935–945.

Chan JK and Lu ML (2007) An efficient algorithm for Aeolian vibration of single conductor with multiple dampers. *Institute of Electrical and Electronics Engineers, Transactions on Power Delivery* 22(3): 1822–1829.

Claren R and Diana G (1969) Mathematical analysis of transmission line vibration. *Institute of Electrical and Electronics Engineers, Transactions on Power Apparatus and Systems* 60(2): 1741–1771.

Dhotard MS, Ganesan N and Rao BVA (1978) Transmission line vibration. *Journal of Sound and Vibration* 60(2): 217–237.

Foda MA (2009) Control of lateral vibrations and slopes at desired locations along vibrating beams. *Journal of Vibration and Control* 15(11): 1649–1678.

Foda MA (2013) Transverse vibration control of translating visco-elastically connected double-string-like continua. *Journal of Vibration and Control* 19(9): 1316–1332.

Kraus M and Hagedorn P (1991) Aeolian vibration: Wind energy input evaluated from measurements on an energized transmission lines. *Institute of Electrical and Electronics Engineers, Transactions on Power Delivery* 6(3): 1264–1270.

Nigol O and Houston HJ (1985) Aeolian vibration of single conductor and its control. *Institute of Electrical and Electronics Engineers, Transactions on Power Apparatus and Systems* 104(11): 3245–3254.

Oguamanam DCD, Hansen JS and Heppler GR (1998) Vibration of arbitrarily oriented two-member open frames with tip mass. *Journal of Sound and Vibration* 209(4): 651–669.

Oniszczuk Z (2000) Free transverse vibration of elastically connected simply supported double-beam complex system. *Journal of Sound and Vibration* 232: 387–403.

Oniszczuk Z (2003) Forced transverse vibrations of an elastically connected complex simply supported double-beam system. *Journal of Sound and Vibration* 264: 273–286.

Palmeri A and Adhikari S (2011) A Galerkin-type state-space approach for transverse vibrations of slender double-beam systems with viscoelastic inner layer. *Journal of Sound and Vibration* 330: 6372–6386.

Vecchiarelly J, Curries IG and Havard DG (2000) Computational analysis of Aeolian conductor vibration with a Stockbridge-type damper. *Journal of Fluid and Structures* 14: 489–509.

Verma H and Hagerdorn P (2004) Wind induced vibration of long electrical overhead transmission line spans: A modified approach. *Journal of Wind and Structures* 8(2): 89–106.

Vu HV, Ordonez AM and Karnopp BH (2000) Vibration of a double-beam system. *Journal of Sound and Vibration* 229(4): 807–882.

Yamaguchi H (1984) Vibration of a beam with an absorber consisting of a viscoelastic beam and a spring-viscous damper. *Journal of Sound and Vibration* 103(3): 417–425.

Appendix

For the sake of simplicity, the following notation is used:

$$
\begin{aligned}
s_{\mathrm{i}} &= \sin \alpha L_{\mathrm{c_i}}, & sh_{\mathrm{i}} &= \sinh \beta L_{\mathrm{c_i}} \\
c_{\mathrm{i}} &= \cos \alpha L_{\mathrm{c_i}}, & ch_{\mathrm{i}} &= \cosh \beta L_{\mathrm{c_i}} \\
s_{\Omega i} &= \sin \Omega_{\mathrm{m}} L_{\mathrm{m_i}}, & sh_{\Omega i} &= \sinh \Omega_{\mathrm{m}} L_{\mathrm{m_i}} \\
c_{\Omega i} &= \cos \Omega_{\mathrm{m}} L_{\mathrm{m_i}}, & ch_{\Omega i} &= \sinh \Omega_{\mathrm{m}} L_{\mathrm{m_i}}
\end{aligned}
$$

Matrix $[\mathcal{F}_{\mathrm{i,j}}]$ comprises 144 elements in which 80 are zero entries and the remaining 64 elements are given as

$$\mathcal{F}_{1,1} = s_1, \quad \mathcal{F}_{1,2} = sh_1, \quad \mathcal{F}_{1,3} = -s_2, \quad \mathcal{F}_{1,1} = -sh_2$$

$$\mathcal{F}_{2,1} = \alpha c_1, \quad \mathcal{F}_{2,2} = \beta ch_1, \quad \mathcal{F}_{2,3} = \alpha c_2, \quad \mathcal{F}_{2,4} = \beta ch_2$$

$$\mathcal{F}_{3,1} = \alpha c_1 h^2 \left(m_1 + m_2 + m_{\mathrm{m_1}} + m_{\mathrm{m_2}}\right) + \frac{\alpha^2}{\omega^2} E_{\mathrm{c}} I_{\mathrm{c}} s_1$$

$$\mathcal{F}_{3,2} = \beta ch_1 h^2 \left(m_1 + m_2 + m_{\mathrm{m_1}} + m_{\mathrm{m_2}}\right) - \frac{\beta^2}{\omega^2} E_{\mathrm{c}} I_{\mathrm{c}} sh_1$$

$$\mathcal{F}_{3,3} = -\frac{\alpha^2}{\omega^2} s_2 E_c I_c, \quad \mathcal{F}_{3,4} = \frac{\beta^2}{\omega^2} sh_2 E_c I_c$$

$$\mathcal{F}_{3,5} = m_1 L_{m_1} s_{\Omega 1} + \Omega_m c_{\Omega 1} I_1 + m_m \left(-\frac{L_{m_1} c_{\Omega 1}}{\Omega_m} + \frac{1}{\Omega_m^2} s_{\Omega 1} \right)$$

$$\mathcal{F}_{3,6} = m_1 L_{m_1} c_{\Omega 1} - \Omega_m s_{\Omega 1} I_1 + m_m \left(\frac{L_{m_1} s_{\Omega 1}}{\Omega_m} + \frac{1}{\Omega_m^2} (c_{\Omega 1} - 1) \right)$$

$$\mathcal{F}_{3,7} = m_1 L_{m_1} sh_{\Omega 1} + \Omega_m ch_{\Omega 1} I_1 + m_m \left(\frac{L_{m_1} ch_{\Omega 1}}{\Omega_m} - \frac{1}{\Omega_m^2} sh_{\Omega 1} \right)$$

$$\mathcal{F}_{3,8} = m_1 L_{m_1} ch_{\Omega 1} + \Omega_m sh_{\Omega 1} I_1 + m_m \left(\frac{L_{m_1} sh_{\Omega 1}}{\Omega_m} - \frac{1}{\Omega_m^2} (ch_{\Omega 1} - 1) \right)$$

$$\mathcal{F}_{3,9} = -m_2 L_{m_2} s_{\Omega 2} - \Omega_m c_{\Omega 2} I_2 - m_m \left(-\frac{L_{m_2} c_{\Omega 2}}{\Omega_m} + \frac{1}{\Omega_m^2} s_{\Omega 2} \right)$$

$$\mathcal{F}_{3,10} = -m_2 L_{m_2} c_{\Omega 2} + \Omega_m s_{\Omega 2} I_2 - m_m \left(\frac{L_{m_2} s_{\Omega 2}}{\Omega_m} + \frac{1}{\Omega_m^2} (c_{\Omega 2} - 1) \right)$$

$$\mathcal{F}_{3,11} = -m_2 L_{m_2} sh_{\Omega 2} - \Omega_m ch_{\Omega 2} I_2 - m_m \left(\frac{L_{m_2} ch_{\Omega 2}}{\Omega_m} - \frac{1}{\Omega_m^2} sh_{\Omega 2} \right)$$

$$\mathcal{F}_{3,12} = -m_2 L_{m_2} ch_{\Omega 2} - \Omega_m sh_{\Omega 2} I_2 - m_m \left(\frac{L_{m_2} sh_{\Omega 2}}{\Omega_m} - \frac{1}{\Omega_m^2} (ch_{\Omega 2} - 1) \right)$$

$$\mathcal{F}_{4,1} = \frac{-\alpha^3}{\omega^2} c_1 E_c I_c, \quad \mathcal{F}_{4,2} = \frac{\beta^3}{\omega^2} ch_1 E_c I_c$$

$$\mathcal{F}_{4,3} = \frac{-\alpha^3}{\omega^2} c_2 E_c I_c, \quad \mathcal{F}_{4,4} = \frac{\beta^3}{\omega^2} ch_2 E_c I_c$$

$$\mathcal{F}_{4,5} = m_1 s_{\Omega 1} - \frac{m_m}{\Omega_m} (c_{\Omega 1} - 1), \quad \mathcal{F}_{4,6} = m_1 c_{\Omega 1} + \frac{m_m}{\Omega_m} s_{\Omega 1}$$

$$\mathcal{F}_{4,7} = m_1 sh_{\Omega 1} + \frac{m_m}{\Omega_m} (ch_{\Omega 1} - 1), \quad \mathcal{F}_{4,8} = m_1 ch_{\Omega 1} + \frac{m_m}{\Omega_m} sh_{\Omega 1}$$

$$\mathcal{F}_{4,9} = m_2 s_{\Omega 2} - \frac{m_m}{\Omega_m} (c_{\Omega 2} - 1), \quad \mathcal{F}_{4,10} = m_2 c_{\Omega 2} + \frac{m_m}{\Omega_m} s_{\Omega 2}$$

$$\mathcal{F}_{4,11} = m_2 sh_{\Omega 2} + \frac{m_m}{\Omega_m} (ch_{\Omega 2} - 1), \quad \mathcal{F}_{4,12} = m_2 ch_{\Omega 2} + \frac{m_m}{\Omega_m} sh_{\Omega 2}$$

$$\mathcal{F}_{5,5} = s_{\Omega 1} - \lambda_{m_1} \Omega_m^3 c_{\Omega 1}, \quad \mathcal{F}_{5,6} = c_{\Omega 1} + \lambda_{m_1} \Omega_m^3 s_{\Omega 1}$$

$$\mathcal{F}_{5,7} = sh_{\Omega 1} + \lambda_{m_1} \Omega_m^3 ch_{\Omega 1}, \quad \mathcal{F}_{5,8} = ch_{\Omega 1} + \lambda_{m_1} \Omega_m^3 sh_{\Omega 1}$$

$$\mathcal{F}_{6,9} = s_{\Omega 2} - \lambda_{m_2} \Omega_m^3 c_{\Omega 2}, \quad \mathcal{F}_{6,10} = c_{\Omega 2} + \lambda_{m_2} \Omega_m^3 s_{\Omega 2}$$

$$\mathcal{F}_{6,11} = sh_{\Omega 2} + \lambda_{m_2} \Omega_m^3 ch_{\Omega 2}, \quad \mathcal{F}_{6,12} = ch_{\Omega 2} + \lambda_{m_2} \Omega_m^3 sh_{\Omega 2}$$

$$\mathcal{F}_{7,5} = c_{\Omega 1} + \kappa_{m_1} \Omega_m s_{\Omega 1}, \quad \mathcal{F}_{7,6} = -s_{\Omega 1} + \kappa_{m_1} \Omega_m c_{\Omega 1}$$

$$\mathcal{F}_{7,7} = ch_{\Omega 1} - \kappa_{m_1} \Omega_m sh_{\Omega 1}, \quad \mathcal{F}_{7,8} = sh_{\Omega 1} - \kappa_{m_1} \Omega_m ch_{\Omega 1}$$

$$\mathcal{F}_{8,9} = c_{\Omega 2} + \kappa_{m_2} \Omega_m s_{\Omega 2}, \quad \mathcal{F}_{8,10} = -s_{\Omega 2} + \kappa_{m_2} \Omega_m c_{\Omega 2}$$

$$\mathcal{F}_{8,11} = ch_{\Omega 2} - \kappa_{m_2} \Omega_m sh_{\Omega 2}, \quad \mathcal{F}_{8,12} = sh_{\Omega 2} - \kappa_{m_2} \Omega_m ch_{\Omega 2}$$

$$\mathcal{F}_{9,1} = \mathcal{F}_{10,1} = -s_1, \quad \mathcal{F}_{9,2} = \mathcal{F}_{10,2} = -sh_1$$

$$\mathcal{F}_{9,6} = \mathcal{F}_{9,8} = \mathcal{F}_{10,10} = \mathcal{F}_{10,12} = 1$$

$$\mathcal{F}_{11,1} = \frac{-\alpha c_1}{\Omega_m}, \quad \mathcal{F}_{11,2} = \frac{-\beta ch_1}{\Omega_m}$$

$$\mathcal{F}_{12,1} = -\mathcal{F}_{11,1}, \quad \mathcal{F}_{12,2} = -\mathcal{F}_{11,2}$$